The following publication H. Xue, J. Mahseredjian, J. Morales and I. Kocar, "Analysis of Cross-Bonded Cables Using Accurate Model Parameters," in IEEE Transactions on Power Delivery, vol. 38, no. 1, pp. 46-55, Feb. 2023 is available at https://doi.org/10.1109/TPWRD.2022.3179832

Analysis of Cross-Bonded Cables Using Accurate Model Parameters

Haoyan Xue, *Senior Member, IEEE*, Jean Mahseredjian, *Fellow, IEEE,* Jesus Morales*, Member, IEEE* and Ilhan Kocar, *Senior Member, IEEE*

***Abstract*—This paper presents a thorough investigation of frequency and electromagnetic transient (EMT) responses of cross-bonded cables. The study adopts newly developed Line/ Cable Data (LCD) Module in an existing EMT-type simulation software. The input impedances evaluated by positive sequence and various mode energizations on a typical cross-bonded cable (CBC) in frequency domain are investigated. In addition to cross-bonded, the solid-bonded cable (SBC) and core-transposed cable (CTC) are analyzed for characteristics of input impedance. The mixed propagation modes of CBC and CTC are studied. The influence of bonding methods and cable models on transient voltages is investigated. The results simulated by the new LCD are compared with the Classical Parameter Calculation (CPC) method and validated by recently proposed extended transmission line (ETL) approach.**

***Index Terms*— Cross-bonded cable, Line / Cable Data, input impedance, cable model, electromagnetic transients**

I. Introduction

THE sheath cross-bonding technique on a three-phase single core cable has been used in underground high voltage power delivery since several decades [1]-[3]. The different bonding methods with grounding resistance play an important role in reducing losses and overvoltages on cable sheath. Since the bonding point within a major section and the connection point between each major section create discontinuities for electromagnetic wave propagations, it relies on electromagnetic transient (EMT) type simulation software [4] to analyze the complicated transient characteristics of cross-bonded cables.

The investigations of steady-state and transient responses on various bonded cables using circuit theory together with adoption of traveling wave analysis and Fourier transformation are performed since the 1960s [5]-[22]. Moreover, a homogeneous model has been proposed to approximately represent a non-homogeneous major section in a cross-bonded cable (CBC) [15], [16]. The homogeneous model has considerably better computational efficiency for the long CBC.

The EMT-type simulation tools with advanced cable models have become powerful tools in analysis of transient states of large high voltage AC cable networks [1], [2]. In general, the cable models used in transient studies rely on classical routines of Line Constants [23] and Cable Constants [24], [25] to acquire longitudinal and shunt per-unit-length (p.u.l) parameters.

In addition, a multi-conductor analysis method has been proposed in [35] for analysis of steady-state in bridge installed cable, and the method has been further improved for study of steady-state with submarine cable [36].

None of the above studies are based on the latest techniques [26]-[34] which include more accurate expressions for the calculation of external parameters on various bonding cables in EMT study. This fact constitutes the centerpiece of this paper.

In Section II, of this paper, three generic CBC models used in an EMT-type software (EMTP) [37], are introduced, i.e. detailed and homogeneous models. The series and shunt parameters used in the cable models are evaluated using the recently developed new Line / Cable Data (LCD) Module [26]-[34].

Section III performs the frequency domain study on cable input impedance for various bonding methods with the Exact-PI model [1]. The CBC, solid-bonded cable (SBC) and core-transposed cable (CTC) are discussed. The responses of input impedance for positive sequence and different mode energizations are investigated in detail. The characteristics of mixed propagation modes of CBC and CTC, the impact of length of CBC, the influence of different bonding ways (CBC, SBC and CTC) and grounding resistance are analyzed using the new LCD and Classical Parameter Calculation (CPC) [23]-[25] methods.

In Section IV, typical CBC, SBC and CTC are adopted into transient simulations using the Wideband (WB) model [38]. The maximum sheath voltages on different major sections and behaviors of detailed and homogenous models are investigated.

The new LCD is capable of accounting for overhead lines, underground cables, mutual couplings between overhead and underground conductors together with a consideration of multi-layer earth, stranded conductors, proximity effect, high frequency transient and complete expression of earth-return parameters, etc. Recent research [28], [39] shows that the abnormal characteristics of input impedance and propagation constant produced by CPC method may cause passivity violation in numerical fitting of the WB model, and it could further lead to simulation instability. The LCD avoids such problems and provides a new tool to researchers and engineers for accurate simulation of cables and lines in power grids.

Moreover, all the results calculated in frequency and transient domains are validated using the extended transmission line (ETL) [26] approach. It should be noted that the

H. Xue and J. Mahseredjian are with Polytechnique Montréal, J. Morales is with PGSTech, Canada, and I. Kocar is with the Hong Kong Polytechnic University (e-mail: haoyan.xue@polymtl.ca, jeanm@polymtl.ca, jesus.morales@emtp.com, ilhan.kocar@polyu.edu.hk).

effectiveness of the ETL approach presented in [26] and [40], has been thoroughly validated by adopting the Method of Moments (MoM) in frequency-domain [30], [41] and Finite-Difference Time-Domain (FDTD) in time-domain [42].

The novel features of the new LCD module can be used to fundamentally replace existing parameters calculation methods (CPC). This is an important new information in practices for the simulation of EMTs with cables.

II. Typical Models of CBC in Transient Simulations

A. Detailed model of a major section

Fig. 1 illustrates a major section of a CBC, and it can be represented by Exact-PI or WB model in EMTP depending on the investigation's objective. The Exact-PI and WB models are adopted in the frequency scan and transient simulations in Section III and Section IV. Each major section consists of three minor sections. The p.u.l parameters of the minor section are evaluated by new LCD and ETL methods.

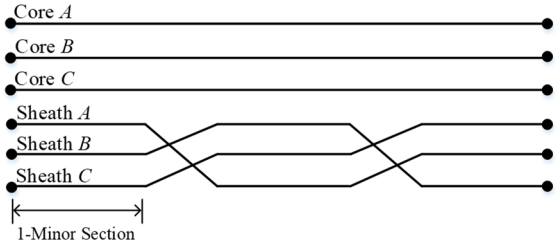

(a) CBC

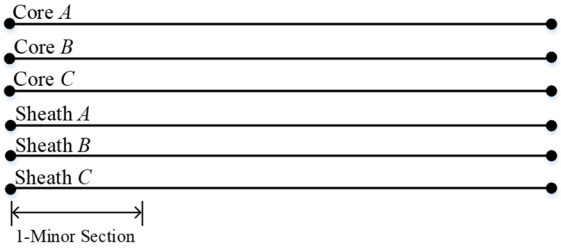

(b) SBC

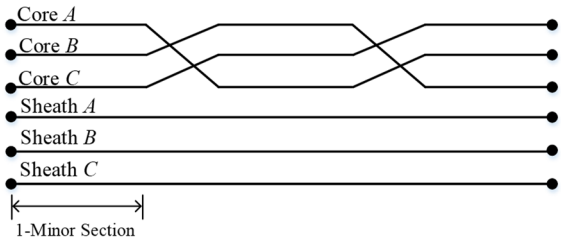

(c) CTC

Fig. 1 Detailed model for a major section for various cables in EMTP.

B. Homogeneous models of a major section

In general, a major section of CBC may have non-homogeneous characteristics which mean different lengths for minor sections. It is possible to approximately represent a major section shown in Fig. 1 by three identical minor sections using the lumped parameters. Thus, if a major section is non-homogeneous, the following expressions of parameters [1]-[3] can be used to model it in EMTP.

$$\mathbf{Z_m} = \frac{1}{3}\left(\mathbf{Z} + \mathbf{A_R Z A_R^{-1}} + \mathbf{A_R^{-1} Z A_R}\right) \tag{1}$$

$$\mathbf{Y_m} = \frac{1}{3}\left(\mathbf{Y} + \mathbf{A_R Y A_R^{-1}} + \mathbf{A_R^{-1} Y A_R}\right) \tag{2}$$

where $\mathbf{Z}$ and $\mathbf{Y}$ represent p.u.l impedance and admittance matrices of a minor section, and both can be calculated by CPC, new LCD and ETL methods. $\mathbf{A_R}$ is a rotational matrix due to various bonding methods in a major section [1]-[3].

Next, the following relations [1] can be obtained to further reduce the matrix orders of (1) and (2) from 6-by-6 to 4-by-4.

$$\mathbf{Z_{mh}} = \left(\mathbf{T Z_m T^t}\right)^{-1} \tag{3}$$

$$\mathbf{Y_{mh}} = \mathbf{T Y_m T^t} \tag{4}$$

where transformation matrix $\mathbf{T}$ is given in [1]-[3].

As shown in Fig. 2 (a), a major section can be modeled by adopting (3) and (4) into EMTP using Exact-PI or WB model.

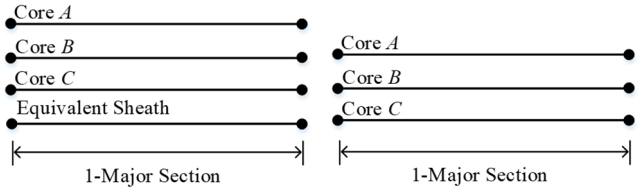

(a) Homogeneous model 1 (b) Homogeneous model 2

Fig. 2 Homogeneous models of a major section in CBC.

Furthermore, the three phase sheaths can be assumed to be continuously grounded and eliminated using reduction logic which is similar to grounding wires of overhead lines, then only three cores are left, as illustrated in Fig. 2 (b).

C. Parameters and configuration of cable

Fig. 3 illustrates a three phase single core cable which has been adopted into the investigations of Sections III and IV. The parameters and geometrical data are found in [1], [2].

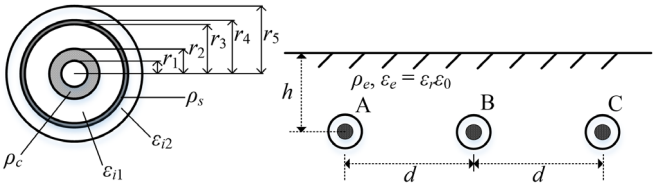

(a) Geometrical parameters (b) Configuration

Fig. 3 Data of three phase single core cable.

III. Frequency Domain Studies

In this frequency domain study, the length of a major section in CBC, SBC and CTC is 788 m. The three minor sections are set to 263 m, 323 m and 202 m, respectively [1], [2]. The cable configuration is given in Fig. 3 with resistivity and relative permittivity of earth assumed to be 100 Ωm and 1.

The Exact-PI model is used in this section.

A. Positive sequence energization

The positive sequence energization on a CBC, SBC and CTC with *N*-major sections is shown in Fig. 4. The current amplitudes and phase angles are given by: $I_A = 1\angle 0°$, $I_B = 1\angle -120°$ and $I_C = 1\angle 120°$. The cable sheath at each end of major section is grounded by $R_g = 10\,\Omega$.

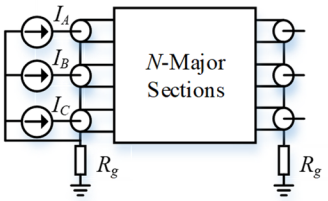

Fig. 4 Positive sequence energization on a CBC, SBC and CTC.

1) Mixed wave propagation of cross-bonded cable

The absolute value of input impedance $|Z_{in}|$ calculated using CBC with 1-major section based on positive sequence energization is illustrated in Fig. 5. The input impedance calculated by CPC shows high frequency spikes if frequency is above 30 kHz. However, the results produced by new LCD and ETL remain smooth as frequency increases.

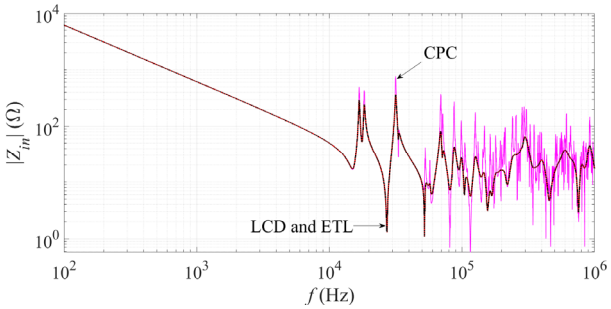

Fig. 5 Input impedance of CBC, 1-major section.

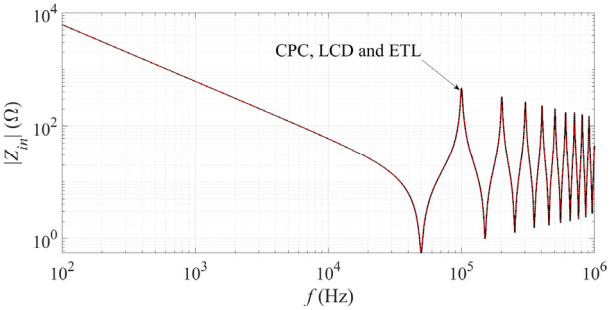

Fig. 6 Input impedance of SBC, 1-major section.

Fig. 6 illustrates the $|Z_{in}|$ evaluated as in Fig. 5, except that the cable is now solidly bonded for a major section. Significant differences are observed in comparison to results in Fig. 5. Firstly, the new LCD and ETL methods have no effect on characteristics of input impedance. Next, a periodical oscillations of input impedance occurs, i.e. zeros at $f = 50.1$ kHz, $f = 150.3$ kHz and $f = 251.8$ kHz etc.

If three cores of the cable are transposed and the sheath is solidly bonded within a major section, the impedance scan is illustrated in Fig. 7. Similar to the CBC, the new LCD and ETL methods have significant impact on the calculated results in the high frequency region.

In fact, the phenomena observed in Fig. 5 to Fig. 7 involve complicated mixed mode propagation of CBC and CTC, as discussed in [2], [15]. However, these references are based on the CPC method and cannot explain the observations made with new LCD and ETL methods. Moreover, the modal analysis is adopted below to elaborate the phenomena observed in Fig. 5 to Fig. 7.

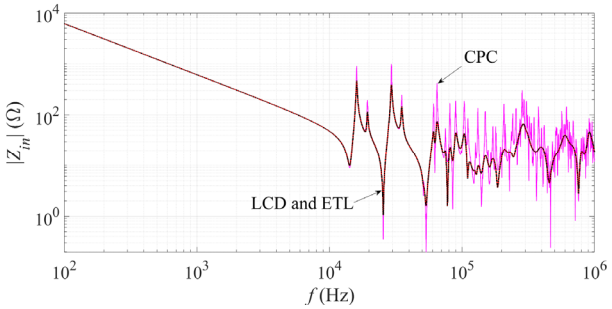

Fig. 7 Input impedance of CTC, 1-major section.

First of all, the current transformation matrices (5) to (7) are calculated using the homogeneous equations (1) and (2) based on three different bonding methods at $f = 100$ kHz. Although (1) and (2) are homogeneous approximations to a non-homogenous major section of cable, it is enough to explain the mixed mode propagation. The series and shunt parameters of minor section are produced by new LCD and verified by ETL. The matrices of parameters follow the Core - Sheath sequence shown in Fig. 1.

Next, the first three columns of (5) to (7) represent propagation modes of earth-return and inter-sheath. Three pure co-axial modes for SBC or a pure co-axial mode and two inter-core modes for CBC and CTC are given in the last three columns of (5) to (7). The rows of matrices (5) to (7) follow the sequence of Core *A*, Core *B*, Core *C*, Sheath *A*, Sheath *B* and Sheath *C*. Also, the modal propagation constants calculated at $f = 100$ kHz using new LCD are shown in TABLE I and TABLE II.

$$\mathbf{B}_{\mathrm{CBC}} = \begin{bmatrix} 0 & 0 & 0 & 0.41 & 0.71 & -0.41 \\ 0 & 0 & 0 & 0.41 & 0 & 0.82 \\ 0 & 0 & 0 & 0.41 & -0.71 & -0.41 \\ 0.58 & -0.25 & -0.71 & -0.41 & 0 & 0 \\ 0.58 & 0.64 & 0.71 & -0.41 & 0 & 0 \\ 0.58 & -0.39 & 0 & -0.41 & 0 & 0 \end{bmatrix} \quad (5)$$

$$\mathbf{B}_{\mathrm{SBC}} = \begin{bmatrix} 0 & 0 & 0 & -0.29 & -0.5 & 0.4 \\ 0 & 0 & 0 & 0.56 & 0 & 0.42 \\ 0 & 0 & 0 & -0.29 & 0.5 & 0.4 \\ 0.57 & -0.71 & -0.41 & 0.29 & 0.5 & -0.4 \\ 0.59 & 0 & 0.82 & -0.56 & 0 & -0.42 \\ 0.57 & 0.71 & -0.41 & 0.29 & -0.5 & -0.4 \end{bmatrix} \quad (6)$$

$$\mathbf{B}_{\mathrm{CTC}} = \begin{bmatrix} 0 & 0 & 0 & 0.41 & 0.82 & -0.17 \\ 0 & 0 & 0 & 0.41 & -0.41 & 0.77 \\ 0 & 0 & 0 & 0.41 & -0.41 & -0.6 \\ 0.56 & -0.41 & 0.71 & -0.41 & 0 & 0 \\ 0.61 & 0.82 & 0 & -0.41 & 0 & 0 \\ 0.56 & -0.41 & -0.71 & -0.41 & 0 & 0 \end{bmatrix} \quad (7)$$

TABLE I MODAL ATTENUATION CONSTANTS, AT 100 KHZ (NP/KM)

Mode (Column in **B**)	1	2	3	4	5	6
CBC	12.13	0.569	0.569	0.052	0.038	0.043
SBC	12.13	0.779	0.449	0.052	0.052	0.052
CTC	12.13	0.43	0.73	0.052	0.039	0.039

TABLE II MODAL PHASE VELOCITY, AT 100 KHZ (m/μs)

Mode (Column in **B**)	1	2	3	4	5	6
CBC	14.15	28.18	28.18	158.12	65.95	76.89
SBC	14.15	27.67	33.54	158.12	158.12	158.12
CTC	14.15	31.34	25.86	158.12	70.75	70.75

Then, the following findings can be summarized to explain the regular, non-regular and spike-like characteristics shown in Fig. 5 to Fig. 7.

- The columns 4 to 6 in (6) with modal propagation constants (modes 4 to 6) in TABLE I and TABLE II show that the SBC involves three pure single-phase co-axial propagation modes within 1-major section. For example, the elements $(1,5)$ and $(4,5)$ in (6) represent the core and sheath of phase *A* with a return negative sign.
- Due to pure co-axial modes appeared in the SBC, the new LCD and ETL show the same results as the CPC method in Fig. 6, since the earth-return admittance implemented into new LCD and ETL has no impact on co-axial modes.
- If the cable is cross-bonded or core-transposed within 1-major section, the columns 5 and 6 in (5) and (7) with modal propagation constants (modes 5 to 6) in TABLE I and TABLE II show that the CBC and CTC have two inter-core modes instead of two co-axial modes of SBC in (6). For example, the elements $(1,5)$ and $(3,5)$ in (5) represent the cores of phases *A* and *C* with a return negative sign.
- The inter-core mode produced by CBC and CTC is essentially mixed propagations of co-axial and inter-sheath modes due to flux interactions. Then, it results into the non-regular oscillating waveforms of input impedance calculated by CBC and CTC in comparison to regular oscillations obtained by SBC.
- The CPC method produces dense spike-like noises of input impedance as frequency increases for CBC and CTC, and the essential reason is an impedance mismatching caused by incomplete representation of shunt part in CPC method.
- Although the inter-core mode produced in CBC and CTC is a mixed propagation mode, it is partially dominated by the inter-sheath mode at high frequency. The earth-return admittance has significant influence on the inter-sheath mode of cable, thus the missing of earth-return admittance in shunt parameter of CPC method directly reflects on the abnormal spikes in results of input impedance.

The fundamental oscillating frequency of SBC can be calculated by [1]

$$f_o = \frac{v_c}{4l} = 50.16\,\text{kHz} \tag{8}$$

where v_c is propagation velocity in co-axial mode, and it is given in TABLE II, and l is length of a major section.

Since the cores of far end in Fig. 4 are open-circuited, periodical oscillating frequency of zeros is odd number times than fundamental frequency f_o, and the first two frequencies are

$$f_3 = 3f_o = 150.5\,\text{kHz},\ f_5 = 5f_o = 250.8\,\text{kHz} \tag{9}$$

Equations (8) and (9) accurately match the results shown in Fig. 6 . The fundamental oscillating frequency of inter-sheath mode on CBC can be also evaluated by adopting $v_c = 28.18$ m/μs (see TABLE II) into (8) to result into $f_o = 8.94$ kHz. Thus, the influence of mixture of modes on CBC becomes more visible if the frequency is higher than 8.94 kHz, i.e. $f = 14.89$ kHz in Fig. 5.

Fig. 8 illustrates the calculated $|Z_{in}|$ of CBC using 12-major sections, and other conditions remaining the same as in Fig. 5. The total CBC length becomes 9456 m. The fundamental oscillating frequency of first peak shifts to 3.42 kHz in comparison to 16.79 kHz of cable with 1-major section. Also, the mixed propagation mode is observed. The high frequency spikes are removed if new LCD and ETL methods are adopted into calculations.

As shown in Fig. 9, some minor influences are observed on oscillations of input impedance while the earth resistivity is varied from 10 Ωm to 500 Ωm. Only new LCD is used in the calculations of Fig. 9.

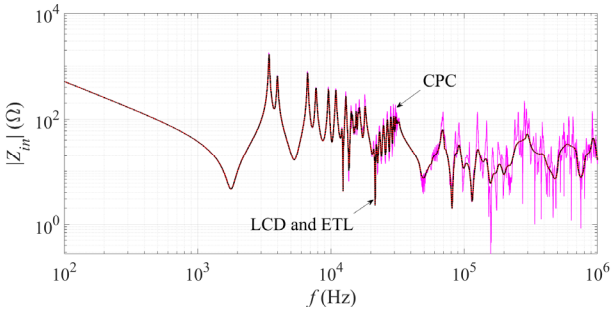

Fig. 8 Input impedance of CBC, 12-major sections.

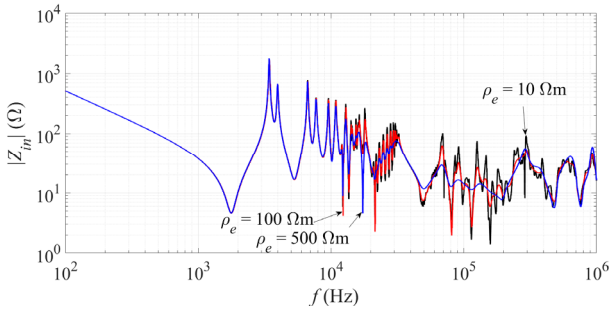

Fig. 9 Input impedance of CBC with different earth resistivities, 12-major sections.

2) Influence of length of CBC

Fig. 10 illustrates the influence of length on calculated input impedance of CBC.

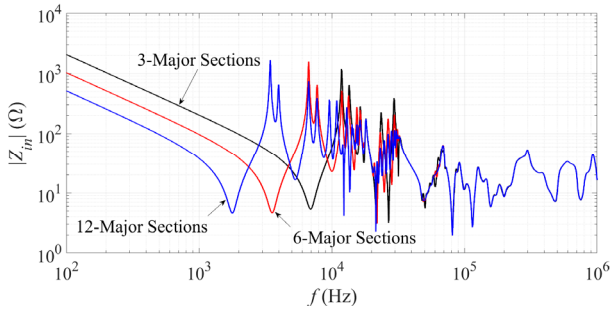

Fig. 10 Input impedance of CBC with 3-, 6- and 12-major sections.

The new LCD method is used in the calculation. The total lengths of cable with 3- and 6- major sections are 2364 m and 4728 m, respectively. The fundamental oscillating frequency decreases as length increases. Moreover, the impact of number of major sections becomes negligible if the frequency is above a breaking point 33.04 kHz.

3) Influence of bonding method

The effects on input impedance of detailed and homogeneous models of CBC shown in Fig. 1 and Fig. 2, respectively, are illustrated in Fig. 11. Also, the cables with 1- and 12- major sections are considered. The cable parameters are calculated by new LCD. It is obvious that the applicable limit of homogeneous modeling methods is up to around 13 kHz. Note that the mixed mode propagation in high frequency cannot be represented by homogeneous methods.

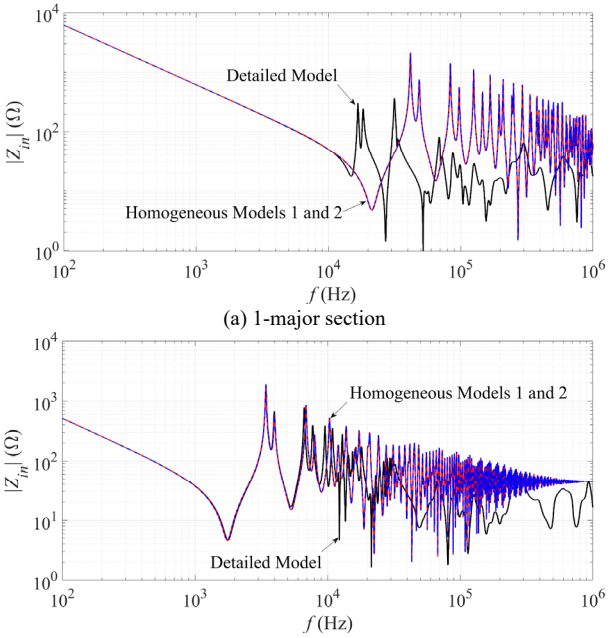

(a) 1-major section

(b) 12-major sections

Fig. 11 Input impedance of CBC calculated by detailed and homogeneous models.

B. Influence of sheath energization

Fig. 12 shows two types of inter-sheath energizations on CBC using *N*-major sections. The current sources are set to $I_A = I_C = -0.5\angle 0°$ and $I_B = 1\angle 0°$ for Fig. 12 (a), and $I_B = 1\angle 0°$, $I_C = -1\angle 0°$ for Fig. 12 (b). $R_g = 10\,\Omega$ is used in the calculations.

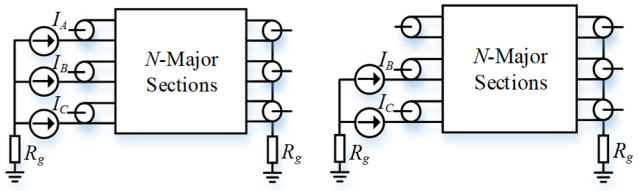

(a) Inter-sheath 1 (b) Inter-sheath 2

Fig. 12 Inter-sheath energizations on a CBC.

The input impedance of CBC excited by inter-sheath 1 is shown in Fig. 13. The impedances obtained by new LCD and ETL are significantly different from results calculated using CPC if frequency is above 50 kHz. The input impedance evaluated by new LCD and ETL converges to a stable value as frequency increases. Also, some minor impedance oscillations are produced by CBC using 12-major sections.

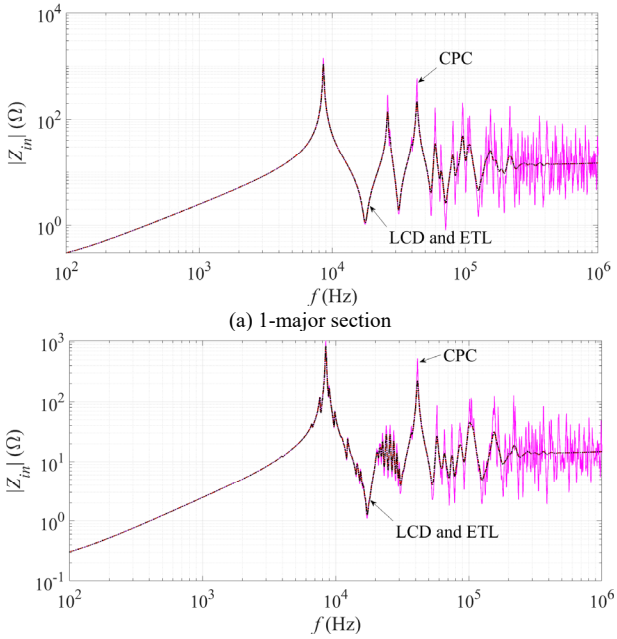

(a) 1-major section

(b) 12-major sections

Fig. 13 Input impedance of CBC excited by energization of inter-sheath 1.

Fig. 14 shows the input impedance calculated by energization of inter-sheath 2. Again, the results produced by new LCD and ETL converge to stable values in high frequency. Also, the impedances calculated by two-phase inter-sheath energization (inter-sheath 2) are similar to the results obtained by three-phase inter-sheath energization (inter-sheath 1).

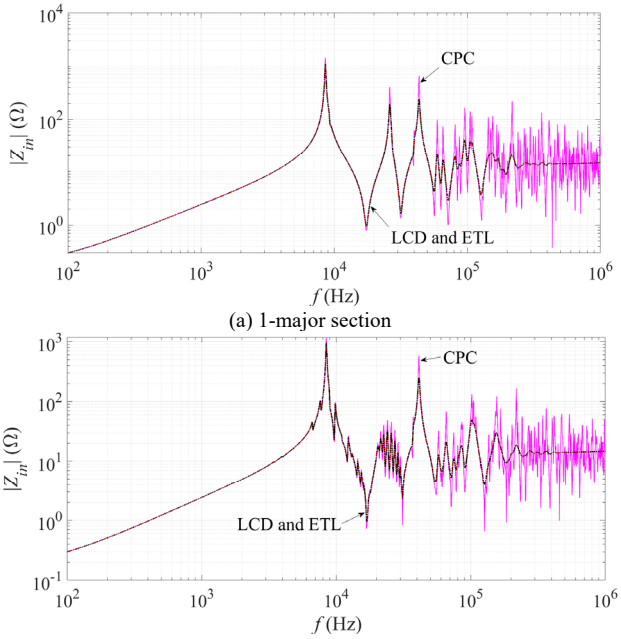

(a) 1-major section

(b) 12-major sections

Fig. 14 Input impedance of CBC excited by energization of inter-sheath 2.

It should be noted that the dense spikes obtained by CPC method in Fig. 13 and Fig. 14 further prove the mixed characteristics of modes shown in Fig. 5 to Fig. 7.

C. Earth-return effect

An earth-return energization on a CBC with *N*-major sections is illustrated in Fig. 15. The current source is set to $I_B = 1\angle 0°$.

Fig. 16 illustrates the $|Z_{in}|$ of CBC excited by earth-return energization. Unlike positive sequence and inter-sheath energizations, the impedance evaluated by earth-return energization shows no spikes in high frequency for CPC, new LCD and ETL methods. The results obtained by new LCD and ETL increase as frequency increases.

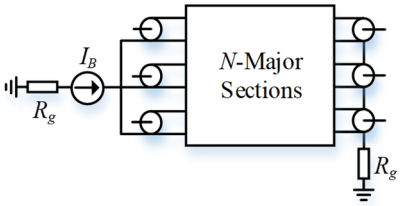

Fig. 15 Earth-return energization on a CBC.

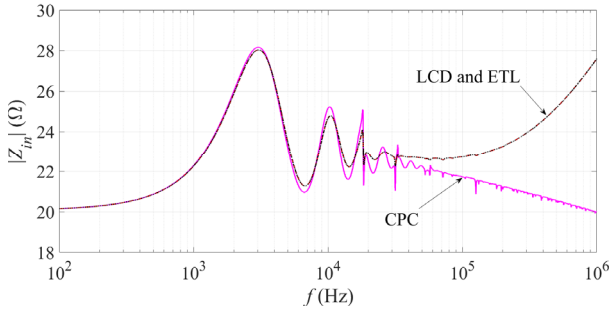

(a) 1-major section

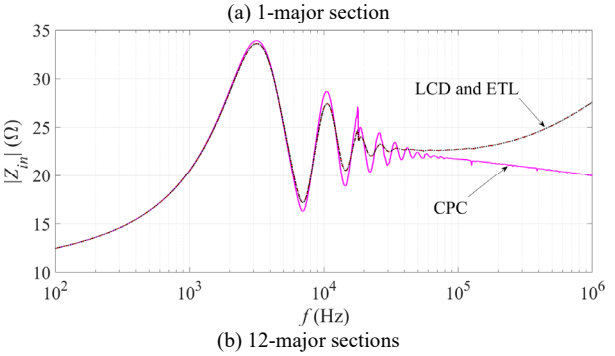

(b) 12-major sections

Fig. 16 Input impedance of CBC excited by earth-return energization.

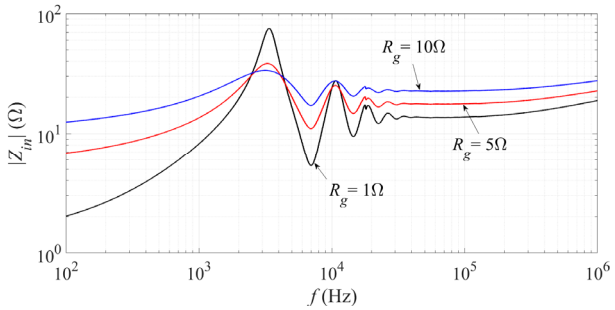

Fig. 17 Influence of grounding resistance on input impedance of earth-return energization.

Fig. 17 shows effect of grounding resistance on input impedance of earth-return energization. The cable is with 12-major sections. The grounding resistance has significant influence on the calculated input impedance. However, the grounding resistance has no visible influence on input impedance calculated by positive sequence and inter-sheath energizations although the results are not shown in this paper.

IV. Time Domain Studies

The transient study is performed in EMTP with its WB model. The energization circuit of CBC, SBC and CTC with *N*-major sections using earth resistivity 100 Ωm and earth relative permittivity 1 is shown in Fig. 18. The AC voltage sources are 60 Hz at 132 kV. The ideal circuit breakers are closed sequentially from phases *A* to *C* at 0 ms, 0.1 ms and 0.2 ms.

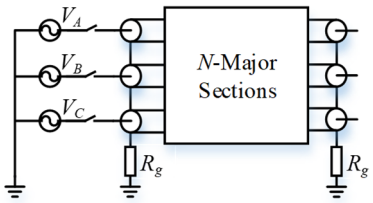

Fig. 18 Three-phase energization on a CBC, SBC and CTC in transient simulations.

A. Influence of bonding methods

The effect of bonding methods, i.e. cross-bonded, solid-bonded and core-transposed on sheath voltage of cable is illustrated in Fig. 19 to Fig. 21. The simulations adopt 12 major sections. R_g is set to 10 Ω.

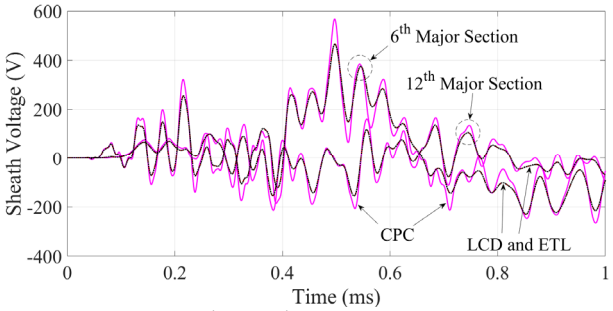

Fig. 19 Sheath voltages at 6th and 12th major sections based on CBC.

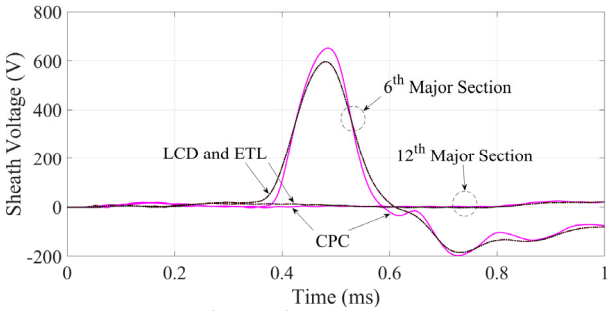

Fig. 20 Sheath voltages at 6th and 12th major sections based on SBC.

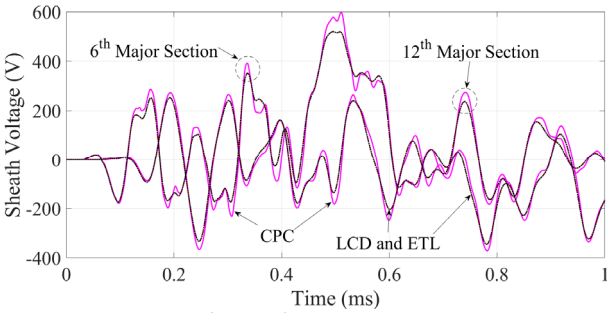

Fig. 21 Sheath voltages at 6th and 12th major sections based on CTC.

The maximum sheath voltages at the 6th and 12th major sections of Fig. 19 to Fig. 21 are summarized in the following table.

TABLE III MAXIMUM SHEATH VOLTAGES SUMMARIZED BASED ON FIG. 19 TO FIG. 21

Methods	Type of Bonding	Sheath Voltage (V)	
		6th Major Section	12th Major Section
CPC	CBC	567.8	-212.5
	SBC	651.6	25.6
	CTC	597.1	-366.1
New LCD / ETL	CBC	465.4	-154.6
	SBC	596.5	22.1
	CTC	515.9	-328.3

As shown in TABLE III, the sheath generally experiences higher overvoltage at the 6th major section than the far end of cable. The sheath voltage at the 12th major section using SBC experiences the least overvoltage. However, it produces the highest sheath overvoltage at the 6th major section.

Moreover, the maximum sheath voltage calculated by CPC shows significant differences in comparison to the results obtained by new LCD and ETL. For example, 22% and 37.5% deviations on maximum sheath voltage of CBC are observed if it is referred to new LCD.

B. Influence of grounding resistance

As shown in Fig. 22, the sheath voltages at the 6th and 12th major section are calculated varying the values of grounding resistance. It is clear that the sheath voltage decreases as grounding resistance decreases. Only new LCD is used in the simulations.

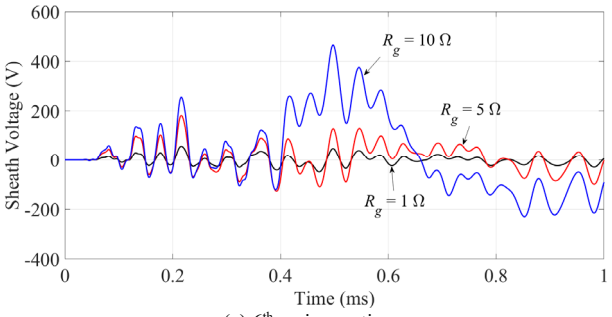

(a) 6th major section

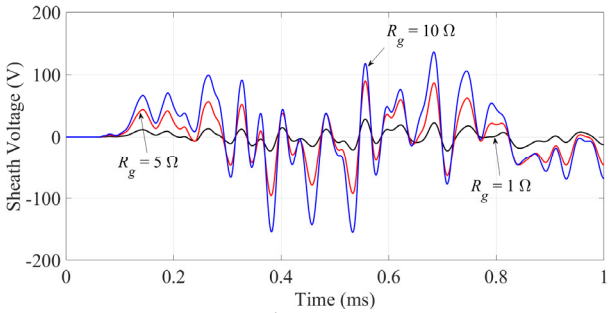

(b) 12th major section

Fig. 22 Influence of grounding resistance on sheath voltage of CBC.

C. Influence of modeling methods

The influence of detailed and homogeneous models on core and sheath transient voltages of CBC is shown in Fig. 23 to Fig. 25. The cable with 1-, 12- and 24- major sections are inspected with $R_g = 10\,\Omega$. The new LCD is used in the simulations.

The results simulated using homogeneous models 1 and 2 on cable with 1-major section show large deviations from waveforms obtained by detailed model.

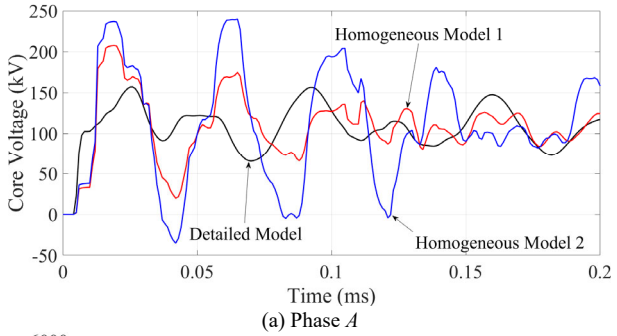

(a) Phase *A*

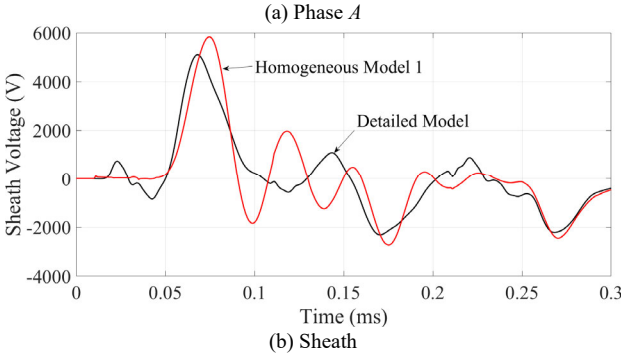

(b) Sheath

Fig. 23 Transient voltages at far end of CBC, 1-major section.

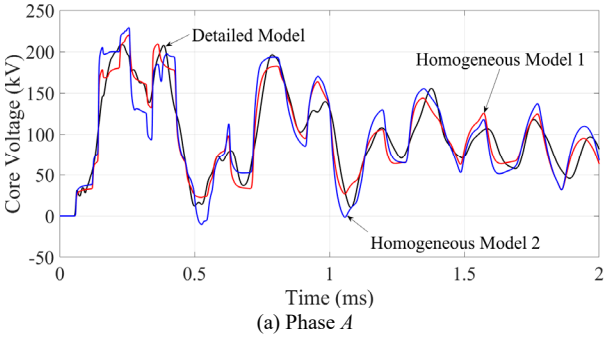

(a) Phase *A*

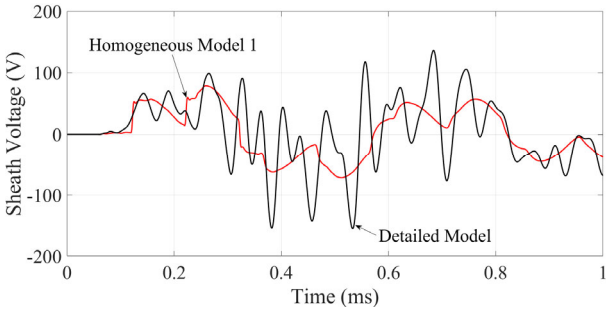

(b) Sheath

Fig. 24 Transient voltages at far end of CBC, 12-major sections.

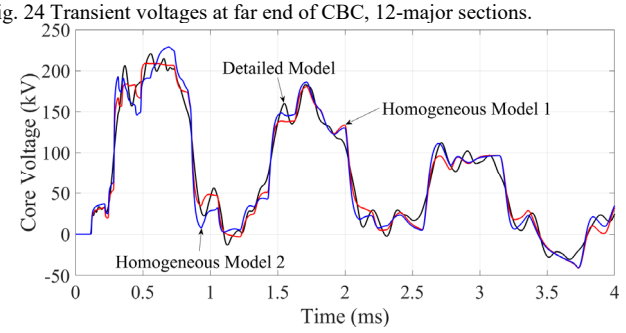

(a) Phase *A*

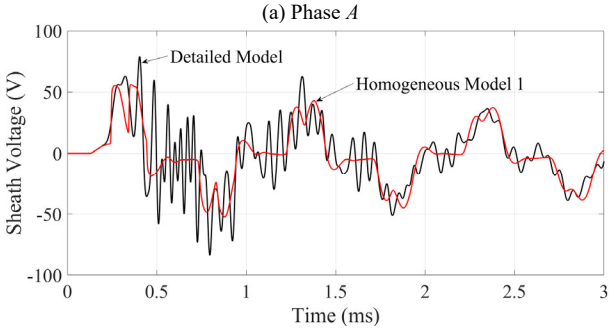

(b) Sheath

Fig. 25 Transient voltages at far end of CBC, 24-major sections.

However, the performance of core voltage is significantly improved if the cable with 12- and 24- major sections are used. The reason is from that the longer cable involves lower dominant frequency, and the homogeneous models with more major sections could shift to their applicable regions as illustrated in Fig. 11. The homogeneous models should be avoided in the analysis of sheath voltages in any cases.

D. Computational performance

The computational performance of EMT simulations using CPC and new LCD methods on the CBC is given in TABLE IV, TABLE V and TABLE VI.

The new LCD method increases CPU computation time in comparison to CPC method if detailed model is used. However, minor differences of CPU time are observed between CPC and new LCD methods for homogeneous models 1 and 2.

Therefore, the homogeneous models would be appropriate solutions for a long and large high voltage cable network due to its high computational efficiency, i.e. 4.9 and 7.8 acceleration ratio for 20- and 50- major sections using homogeneous model 1, 14.5 and 7.5 acceleration ratio for the same number of major sections by adopting homogeneous model 2. However, it is suggested that the similar validations of homogeneous models carried out in the previous sections should be carefully performed in both frequency and transient domains in order to find the application limit.

TABLE IV COMPUTATIONAL TIME OF DETAILED MODEL (SECONDS)

Method	Number of Major Sections					
	1	2	5	10	20	50
CPC	3.2	4	7	12	24	81
New LCD	3.7	5	9	17	36	123

TABLE V COMPUTATIONAL TIME OF HOMOGENEOUS MODEL 1 (SECONDS)

Method	Number of Major Sections					
	1	2	5	10	20	50
CPC	2.5	2.7	3.7	5.1	8.1	17.3
New LCD	2.5	2.7	3.5	4.8	7.4	15.8

TABLE VI COMPUTATIONAL TIME OF HOMOGENEOUS MODEL 2 (SECONDS)

Method	Number of Major Sections					
	1	2	5	10	20	50
CPC	2.3	2.4	2.7	3.3	4.5	7.6
New LCD	2.3	2.4	2.9	3.5	4.8	8.5

V. CONCLUSIONS

This paper performs a thorough investigation of frequency and transient responses of CBC, SBC and CTC by adopting CPC, new LCD and ETL methods. The Exact-PI and Wideband models are used in the simulations of EMTP. It has the following general conclusions.

- In the excitation of positive sequence, the CBC and CTC involve complex mixed propagation modes due to sheath and core phase exchanges within a major section.
- The mixed propagation modes in CBC and CTC are combinations of co-axial and inter-sheath modes.
- In the excitation of positive sequence and inter-sheath modes, the input impedance of CBC and CTC evaluated using CPC method shows dense spike-like noises as frequency increases, however, the results obtained by new LCD have smooth characteristics.
- The essential reason of observed spikes in the calculation of CBC and CTC is impedance mismatching caused by incomplete representation of shunt part in CPC method.
- No spikes are observed for input impedance on CBC and CTC by adopting earth-return energization if the CPC method is used. The input impedance calculated using the new LCD increases as frequency increases, but decreases for the CPC method.
- In general, the sheath voltages evaluated using the new LCD are less than those found by CPC. The maximum deviation of 37.5% on sheath voltages of CBC are observed when referred to new LCD.
- The new LCD increases the CPU simulation time in detailed model of CBC in comparison to the CPU time used by CPC.
- The homogeneous models of CBC have good computational efficiency, however, the model validation in frequency and transient responses should be performed to fit its application region.
- All the results are validated by the ETL approach. The effectiveness of ETL has been studied systematically by MoM and FDTD methods in recent works.
- The effectiveness of the new LCD module has been further verified and confirmed in this paper.

REFERENCES

[1] A. Ametani, T. Ohno and N. Nagaoka, *Cable System Transients: Theory, Modeling and Simulation*, Wiley-IEEE Press, 2015.

[2] A. Ametani, H. Xue, T. Ohno and H. Khalilnezhad, *Electromagnetic Transients in Large HV Cable Networks: Modeling and Calculations*, IET, 2021.

[3] F. F. da Silva and C. L. Bak, *Electromagnetic Transients in Power Cables*, Springer Press, 2013.

[4] A. Ametani (editors), *Numerical Analysis of Power System Transients and Dynamics*, IET, 2015.

[5] E. H. Ball, E. Occhini and G. Luoni, "Sheath overvoltages in high-voltage cables resulting from special sheath-bonding connections," *IEEE Trans. Power App. Syst.*, vol. 84, no. 10, pp. 974-988, 1965.

[6] D. J. Rhodes and A. Wright, "Induced voltages in the sheaths of cross-bonded ac cables," *Proc. Inst. Elect. Eng.*, vol. 113, no. 1, pp. 99-110, 1966.

[7] C. Adamson, E. A.-Z. H. Taha and L. M. Wedepohl, "Comparative steady-state performance of cross-bonded cable systems," *Proc. Inst. Elect. Eng.*, vol. 115, no. 8, pp. 1147-1155, 1968.

[8] A. G. Heaton, "Transient response of cross-bonded cable systems," *Proc. Inst. Elect. Eng.*, vol. 117, no. 3, pp. 578-586, 1970.

[9] L. M. Wedepohl and C. S. Indulkar, "Wave propagation in nonhomogeneous systems: Properties of the chain matrix," *Proc. Inst. Elect. Eng.*, vol. 121, no. 9, pp. 997-1000, 1974.

[10] L. M. Wedepohl and C. S. Indulkar, "Switching overvoltages in short cross-bonded cable systems using the Fourier transform," *Proc. Inst. Elect. Eng.*, vol. 122, no. 11, pp. 1217-1221, 1975.

[11] D. J. Wilcox and K. J. Lawler, "Implementation of nonhomogeneous theory in the transient analysis of cross-bonded cable systems," *Proc. Inst. Elect. Eng.*, vol. 125, no. 10, pp. 993-998, 1978.

[12] W. F. J. Kersten, "Surge arresters for sheath protection in cross-bonded cable system," *Proc. Inst. Elect. Eng.*, vol. 126, no. 12, pp. 1255-1262, 1979.

[13] L. M. Wedepohl and C. S. Indulkar, "Switching overvoltages in long cross-bonded cable systems using the fourier transform," *IEEE Trans. Power App. Syst.*, vol. PAS-98, no. 4, pp. 1476-1480, 1979.

[14] W. D. Humpage, K. P. Wong and T. T. Nguyen, "Z-transform electromagnetic transient analysis of cross-bonded cable transmission systems," *IEE Proc. Gen. Trans. Dist.*, vol. 128, no. 2, pp. 55-62, 1981.

[15] N. Nagaoka and A. Ametani, "Transient calculations on cross-bonded cables", *IEEE Trans. on Power App. Syst.*, vol. PAS-102, no. 4, pp 779-787, 1983.

[16] C. S. Indulkar, P. Kumar and D. P. Kothari "Modal propagation and sensitivity of modal quantities in crossbonded cables," *Proc. Inst. Elect. Eng.*, vol. 130, no. 6, pp. 278-284, 1983.

[17] D. J. Wilcox and K. J. Lawler, "Transient phenomena in cross-bonded cable systems: analytical results," *Proc. Inst. Elect. Eng.*, vol. 125, no. 10, pp. 999-1005, 1978.

[18] U. S. Gudmundsdottir, B. Gustavsen, C. L. Bak, and W. Wiechowski, "Field test and simulation of a 400-kV cross-bonded cable system," *IEEE Trans. Power Delivery*, vol. 26, no. 3, pp. 1403-1410, 2011.

[19] T. Ohno, C. L. Bak, A. Ametani, W. Wiechowski and T. K. Sorensen, "Derivation of theoretical formulas of the frequency component contained in the overvoltage related to long EHV cables," *IEEE Trans. Power Delivery*, vol. 27, no. 2, pp. 866-876, 2012.

[20] I. Lafaia, A. Ametani, J. Mahseredjian, A. Naud, M. T. Correia de Barros and I. Kocar, "Field test and simulation of transients on the RTE 225 kV cable," *IEEE Trans. Power Delivery*, vol. 32, no. 2, pp. 628-637, 2017.

[21] I. Lafaia, A. Ametani, J. Mahseredjian, M. T. Correia de Barros, I. Koçar and Y. Fillion, "Frequency and time domain responses of cross-bonded cables," *IEEE Trans. Power Delivery*, vol. 33, no. 2, pp. 640-648, 2018.

[22] W. Leterme "Y-parameters model of cross-bonded cables including bonding wire impedances," *IEEE Trans. Power Delivery*, vol. 36, no. 1, pp. 495-498, 2021.

[23] H. W. Dommel, *EMTP Theory Book*, Bonneville Power Administration, 1992.

[24] A. Ametani, *Cable Constants*, Bonneville Power Administration, 1976.

[25] A. Ametani, "A general formulation of impedance and admittance of cables," *IEEE Trans. PAS*, vol. PAS-99, pp. 902-910, 1980.

[26] H. Xue, A. Ametani, J. Mahseredjian and I. Kocar, "Generalized formulation of earth-return impedance / admittance and surge analysis on underground cables," *IEEE Trans. Power Delivery*, vol. 33, no.6, pp.2654-2663, 2018.

[27] H. Xue, A. Ametani, J. Mahseredjian, Y. Baba, F. Rachidi and I. Kocar, "Transient responses of overhead cables due to mode transition in high frequencies", *IEEE Trans. Electromag. Compat*, vol. 60, no. 3, pp.785-794, 2018.

[28] H. Xue, A. Ametani and J. Mahseredjian, "Very fast transients in a 500 kV gas - insulated substation," *IEEE Trans. Power Delivery*, vol. 34, no. 2, pp. 627-637, 2019.

[29] H. Xue, A. Ametani, J. Mahseredjian, Y. Baba and F. Rachidi, "Frequency response of electric and magnetic fields of overhead conductors with particular reference to axial electric field," *IEEE Trans. Electromag. Compat*, vol. 60, no. 6, pp. 2029-2032, 2018.

[30] H. Xue, A. Ametani and K. Yamamoto, "Theoretical and NEC calculations of electromagnetic fields generated from a multi-phase underground cable," *IEEE Trans. Power Delivery*, vol. 36, no.3, pp.1270-1280, 2021.

[31] H. Xue, J. Mahseredjian, A. Ametani, J. Morales and I. Kocar, "Generalized formulation and surge analysis on overhead lines: impedance / admittance of a multi-layer earth," *IEEE Trans. Power Delivery*, vol. 36, no. 6, pp. 3834-3845, 2021.

[32] H. Xue, A. Ametani, J. Mahseredjian and I. Kocar, "Computation of overhead line / underground cable parameters with improved MoM - SO method," *Power Systems Computation Conference* (PSCC), Dublin, 2018.

[33] U. R. Patel and P. Triverio, "MoM-SO: a complete method for computing the impedance of cable systems including skin, proximity, and ground return effects," *IEEE Trans. Power Delivery*, vol. 30, pp. 2110-2118, 2014.

[34] U. R. Patel and P. Triverio, "Accurate impedance calculation for underground and submarine power cables using MoM-SO and a multilayer ground model," *IEEE Trans. Power Delivery*, vol. 31, pp. 1233-1241, 2016.

[35] X. Xu, X. Chen, F. Meng and A. Paramane, "Grounding system analysis of 220 kV power cable lines installed underneath a bridge," *IEEE Trans. Power Delivery*, doi: 10.1109/TPWRD.2021.3077620, 2021.

[36] X. Xu, X. Chen, F. Meng and A. Paramane, "Performance of different grounding systems of 500 kV XLPE long submarine cables based on improved multiconductor analysis method," *Electric Power Systems Research*, vol. 202, pp. 1-13, 2022.

[37] J. Mahseredjian, S. Dennetière, L. Dubé, B. Khodabakhchian and L. Gérin-Lajoie, "On a new approach for the simulation of transients in power systems," *Electric Power Systems Research*, vol. 77, no.11, pp. 1514-1520, 2007.

[38] I. Kocar and J. Mahseredjian, "Accurate frequency dependent cable model for electromagnetic transients," *IEEE Trans. Power Delivery*, vol. 31, pp.1281-1288, 2016.

[39] H. Xue, J. Mahseredjian, J. Morales, I. Kocar and A. Xemard, "An investigation of electromagnetic transients for a mixed transmission system with overhead lines and buried cables," *IEEE Trans. Power Delivery*, DOI: 10.1109/TPWRD.2022.3151749, 2022.

[40] T. A. Papadopoulos, D. A. Tsiamitros and G. K. Papagiannis, "Impedances and admittances of underground cables for the homogeneous earth case," *IEEE Trans. Power Delivery*, vol. 25, no. 2, pp. 961-969, 2010.

[41] H. Xue, A. Ametani and K. Yamamoto, "A study on external electromagnetic characteristics of underground cables with considerations of terminations," *IEEE Trans. Power Delivery*, vol. 36, no. 5, pp. 3255-3265, 2021.

[42] N. F. Duarte, A. De Conti and R. Alipio, "Assessment of ground-return impedance and admittance equations for the transient analysis of underground cables using a full-wave FDTD method," *IEEE Trans. Power Delivery*, doi: 10.1109/TPWRD.2021.3131415.